

Discriminating different scenarios to account for the cosmic e^\pm excess by synchrotron and inverse Compton radiation

Juan Zhang¹, Xiao-Jun Bi^{1,2}, Jia Liu³, Si-Ming Liu⁴,

Peng-Fei Yin³, Qiang Yuan¹ and Shou-Hua Zhu³

¹ *Key Laboratory of Particle Astrophysics, Institute of High Energy Physics,*

Chinese Academy of Sciences, Beijing 100049, P. R. China

² *Center for High Energy Physics, Peking University, Beijing 100871, P.R. China*

³ *Institute of Theoretical Physics & State Key Laboratory of Nuclear Physics and Technology,*

Peking University, Beijing 100871, P.R. China

⁴ *Department of Physics and Astronomy, University of Glasgow,*

Kelvin Bldg Rm 620, Glasgow G12 8QQ, United Kingdom

(Dated: February 12, 2022)

The excesses of the cosmic positron fraction recently measured by PAMELA and the electron spectra by ATIC, PPB-BETS, Fermi and H.E.S.S. indicate the existence of primary electron and positron sources. The possible explanations include dark matter annihilation, decay, and astrophysical origin, like pulsars. In this work we show that these three scenarios can all explain the experimental results of the cosmic e^\pm excess. However, it may be difficult to discriminate these different scenarios by the local measurements of electrons and positrons. We propose possible discriminations among these scenarios through the synchrotron and inverse Compton radiation of the primary electrons/positrons from the region close to the Galactic center. Taking typical configurations, we find the three scenarios predict quite different spectra and skymaps of the synchrotron and inverse Compton radiation, though there are relatively large uncertainties. The most prominent differences come from the energy band $10^4 \sim 10^9$ MHz for synchrotron emission and $\gtrsim 10$ GeV for inverse Compton emission. It might be able to discriminate at least the annihilating dark matter scenario from the other two given the high precision synchrotron and diffuse γ -ray skymaps in the future.

PACS numbers: 95.35.+d, 95.85.Ry, 95.85.Pw, 97.60.Gb

I. INTRODUCTION

The anti-matter particles such as positrons and antiprotons in cosmic rays (CRs) are very important in understanding the origin and propagation of CRs. These particles are usually produced by the CR nuclei that interact with the interstellar medium (ISM) when propagating in the interstellar space. Precise measurements of these particles will provide us valuable information about the primary CR sources and the interaction with matter. In addition, these secondary anti-matter particles have relative lower fluxes and characteristic spectra. Therefore they make themselves good objects to study the exotic origin of CRs, such as from dark matter (DM) annihilation or decay.

Recently the PAMELA collaboration released their first CR measurements on the positron fraction [1] and \bar{p}/p ratio [2]. The positron fraction of PAMELA data shows an uprise above ~ 10 GeV till to ~ 100 GeV, which exceeds the background estimation of the conventional CR propagation model. This result is consistent with previous measurements by, e.g., HEAT [3] and AMS [4]. On the other hand, the \bar{p}/p ratio is compatible with the background. The results of PAMELA strongly indicate the existence of such sources that mainly generate leptonic particles at this energy range. The electron spectrum up to several TeV reported by ATIC collaboration also shows an obvious excess with an interesting bump around $300 \sim 800$ GeV [5]. In addition, the measurements of the electron spectrum by PPB-BETS [6], H.E.S.S. [7, 8], and most recently by Fermi [9] all show the excesses of electron spectra, although they are not fully consistent between each other. The studies show that the PAMELA result on the positron fraction is consistent with the electron spectrum measured by ATIC or Fermi assuming the equal amount of the production of positrons and electrons (e.g., [10, 11]).

One possible primary electron/positron source in the Galaxy is the pulsar. Pulsars and their nebulae are well known cosmic particle accelerators. Although the quantitative details of the acceleration processes are still open for study, early radio observations have established them as important high energy cosmic electron and positron sources (e.g., [12]). X-ray and γ -ray observations show that some of the accelerated particles can reach an energy of a few tens of TeV, and there are indications that the particle distribution cuts off in the TeV energy range (e.g., [13, 14, 15]). These particles produce emission over a broadband frequency range in the source region, which has been observed and studied extensively (e.g., [16]). Some of these particles will escape into the ISM becoming high energy cosmic electrons and positrons.

It is shown that one or several nearby pulsars will be able to contribute enough positrons to reproduce the PAMELA data [17, 18] as well as ATIC data [19].

Another potential candidate, which has been widely discussed to solve the positron/electron excess problem, is the DM annihilation (e.g., [20]) or decay (e.g., [21, 22, 23]).

It has been shown in many studies that the local measurements of the electrons/positrons can not provide enough power to discriminate the DM origin and the pulsar origin of the electrons/positrons. On one hand, the ATIC data suggest a sharp cutoff near ~ 600 GeV. Such a feature can naturally appear for a DM origin when closing to the mass of DM particle, if the DM annihilates or decays directly to e^+e^- pair, as shown in Ref. [5]. However, the same thing is also expected if the observed excess is dominated by a single pulsar and/or its nebula and the accelerated high energy electrons and positrons have experienced significant energy loss as they propagate in the source and in the ISM [19]. The narrow peak resulting from local pulsars is even indistinguishable from that of DM origin [24]. On the other hand, if the electron spectrum is as smooth as that from Fermi, there are also degeneracies between the pulsar and DM interpretations. A continuously distributed pulsar population in the Galaxy might be able to generate smoother electron spectrum due to different energy losses of various pulsars. While for the DM scenario, if the electrons and positrons come from DM annihilation or decay, the spectrum can also be smooth, and is consistent with the Fermi measurements [11].

In this work we study the photon emission associated with the different scenarios to see how the degeneracies between these models can be broken. Our point is that although the different scenarios can give almost the same local electrons/positrons, the spatial extrapolations of them might be significantly different, especially in the Galactic center (GC) region. The pulsars mainly concentrate in the Galactic plane, while the DM is spherically distributed in an extended halo and highly concentrated in the center of the halo. In addition, DM annihilation is proportional to $\rho^2(r)$, different from that of DM decay ($\propto \rho(r)$). Therefore we anticipate the existence of remarkable differences in the skymaps of the synchrotron and inverse Compton (IC) emission from these extra primary electrons/positrons for the three scenarios.

We compare the differences of synchrotron as well as IC radiation among the pulsars, annihilating DM and decaying DM models, on the premise that they all reproduce the

positron fraction and total electron + positron flux data. The spectral and directional features of the radiation are discussed in detail. We compare the results with the WMAP haze data [25, 26] and EGRET diffuse γ -ray data [27], and give the observable signals by future experiments such as Fermi/GLAST.

This paper is organized as follows. In Sec. II we will briefly present typical model configurations of the three scenarios which can fit the e^\pm data simultaneously. The discussions on the synchrotron and IC emission are given in Sec. III and IV respectively. In Sec. V we discuss the uncertainties of our predictions. Finally, we give a summary and draw the conclusion in Sec. VI.

II. DIFFERENT SCENARIOS TO ACCOUNT FOR THE e^\pm DATA

We start with the propagation equation of electrons/positrons in the Galaxy

$$\begin{aligned} \frac{\partial \psi}{\partial t} = & Q(\mathbf{r}, p) + \nabla \cdot (D_{xx} \nabla \psi - \mathbf{V}_c \psi) + \frac{\partial}{\partial p} p^2 D_{pp} \frac{\partial}{\partial p} \frac{1}{p^2} \psi \\ & - \frac{\partial}{\partial p} \left[\dot{p} \psi - \frac{p}{3} (\nabla \cdot \mathbf{V}_c \psi) \right], \end{aligned} \quad (1)$$

where ψ is the number density of CR particles per unit momentum interval, $Q(\mathbf{r}, p)$ is the source term, describing the primary particles injected into the interstellar medium, D_{xx} is the spatial diffusion coefficient, \mathbf{V}_c is the convection velocity. The reacceleration process is described by the diffusion in momentum space, with the diffusion coefficient $D_{pp} = \frac{4p^2 v_A^2}{3\delta(4-\delta^2)(4-\delta)wD_{xx}}$, where v_A is the Alfven speed, w is the ratio of magnetohydrodynamic wave energy density to the magnetic field energy density, which characterizes the level of turbulence. $\dot{p} \equiv dp/dt$ is the momentum loss rate, mainly induced by synchrotron radiation and IC scattering for the electrons/positrons for energies $\gtrsim 10$ GeV [28]. In this work, we use the numerical package GALPROP [28] to calculate the propagation of the primary electrons/positrons and the background CRs.

We have adopted the conventional propagation model where all the CR data are reproduced by the model. The cosmic nuclei secondary to primary ratio, such as B/C, the unstable secondary to stable secondary, such as $^{10}\text{Be}/^9\text{Be}$, and the local proton and electron spectra are taken to constrain the propagation parameters. A conventional diffusion + convection (DC) propagation model [22] is adopted. For details of the propagation model see the discussion in Ref. [22]. The propagation parameters are taken as: half height of the propa-

gation halo $z_h = 4$ kpc; diffusion coefficient $D_{xx} = \beta D_0 (\rho/\rho_0)^\delta$ with $D_0 = 2.5 \times 10^{28} \text{ cm}^2 \text{ s}^{-1}$, $\delta = 0.55$ for rigidity $\rho > 4$ GV and $\delta = 0$ for $\rho < 4$ GV; the convection velocity is adopted as a linear function of coordinate z with $V_c(z = 0) = 0$ and $dV_c/dz = 6 \text{ km s}^{-1} \text{ kpc}^{-1}$. The reacceleration is not included.

The source term $Q(\mathbf{r}, p)$ is different for various scenarios. For DM annihilation, the source function of electrons/positrons has the form

$$Q_A(\mathbf{r}, E) = \text{BF} \frac{\langle \sigma v \rangle_A \rho^2(r)}{2 m_{DM}^2} \frac{dN(E)}{dE} \Big|_A, \quad (2)$$

where BF represents the “boost factor” which can come from the clumpiness of DM substructures (e.g., [29, 30, 31]) and/or the so-called Sommerfeld effect [20]. In the former case, BF is energy and spatial dependent, $\text{BF} \sim \text{BF}(\mathbf{r}, E)$. However, the study based on N-body simulations shows that the DM substructures do not tend to strongly enhance the DM annihilation signals [32]. Thus in this work we adopt the Sommerfeld effect as the “boost factor” for discussion. $\langle \sigma v \rangle_A$ is the velocity weighted annihilation cross section before being enhanced by the Sommerfeld effect, m_{DM} is the mass of DM particle, $\frac{dN(E)}{dE} \Big|_A$ is the electron/positron spectrum from one pair of DM annihilation, and $\rho(r)$ is DM density distribution in the Galaxy. To satisfy the relic density constraint we adopt the cross section $\langle \sigma v \rangle_A = 3 \times 10^{26} \text{ cm}^3 \text{ s}^{-1}$. For the DM density profile we adopt the Merritt profile [33]

$$\rho(r) = \rho_0 \exp \left[-\frac{2}{\alpha} \left(\frac{r^\alpha - R_\odot^\alpha}{r_{-2}^\alpha} \right) \right], \quad (3)$$

with $\alpha = 0.2$, $r_{-2} = 25$ kpc and the local DM density $\rho_\odot = 0.3 \text{ GeV cm}^{-3}$ [34] at $r = R_\odot \equiv 8.5 \text{ kpc}$.

For DM decay, the source term is given by

$$Q_D(\mathbf{r}, E) = \frac{1}{\tau_{DM}} \frac{\rho(r)}{m_{DM}} \frac{dN}{dE} \Big|_D, \quad (4)$$

where τ_{DM} is the life time of DM, $\frac{dN}{dE} \Big|_D$ is the electron/positron spectrum from the decay of one DM particle.

The source term for Galactic pulsars is

$$Q_P(R, z, E) = K \cdot f(R, z) \cdot \frac{dN}{dE} \Big|_P, \quad (5)$$

where K is the normalization factor representing the total luminosity of Galactic pulsars, $f(R, z)$ is the pulsar spatial distribution and $\frac{dN}{dE} \Big|_P$ is the average electron/positron energy

spectrum radiated from the pulsars. The spatial distribution of pulsars can be parameterized as

$$f(R, z) \propto \left(\frac{R}{R_\odot}\right)^a \exp\left[-\frac{b(R - R_\odot)}{R_\odot}\right] \exp\left(-\frac{|z|}{z_s}\right), \quad (6)$$

where R is the Galactocentric radius, and z is the distance away from the Galactic Plane. Different from spherically symmetric form of DM distribution, pulsars are mainly concentrated at the Galactic Plane with $z_s \sim 0.2$ kpc. The primary electron/positron spectrum injected by pulsars is generally assumed to be a power law form with an exponential cutoff at high energies

$$\left.\frac{dN}{dE}\right|_P = E^{-\alpha} \exp(-E/E_{cut}), \quad (7)$$

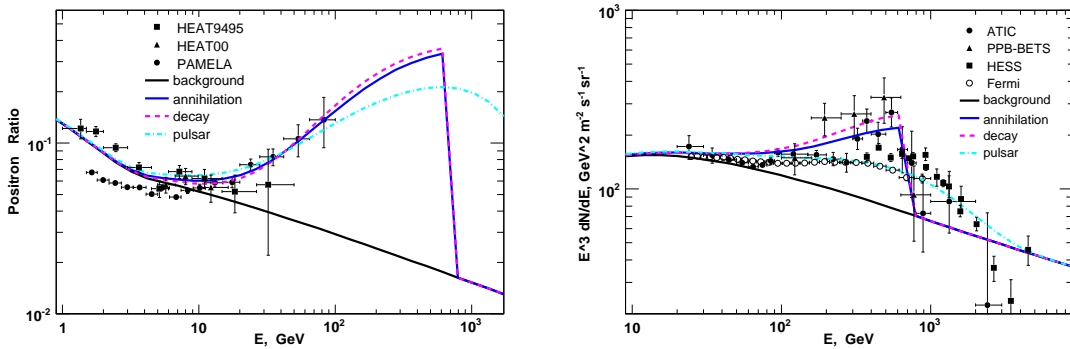


FIG. 1: *Left:* The positron fractions predicted by the three scenarios after solar modulation, compared with HEAT [3, 36] and PAMELA [1] data. *Right:* The total electron+positron fluxes of the three scenarios, compared with observations of ATIC [5], PPB-BETS [6], H.E.S.S. [7, 8] and Fermi [9]. We assume DM annihilates or decays into pure lepton final states with equal branching ratios to e^+e^- , $\mu^+\mu^-$ and $\tau^+\tau^-$.

We have taken appropriate parameters in each scenario to give best fit to the PAMELA and ATIC or Fermi data. For the annihilating DM, we adopt $m_{DM} = 1$ TeV, and a boost factor $BF = 800$. The annihilation channels are assumed to be pure leptons with equal branching ratios to e^+e^- , $\mu^+\mu^-$ and $\tau^+\tau^-$ respectively. We find that the PAMELA and ATIC data can not be fitted well by only one lepton flavor final state. Note, however, for the case of Fermi data the pure $\mu^+\mu^-$ or $\tau^+\tau^-$ channel might be able to fit the data. We will further discuss this point in Sec. V. For the decaying DM, we set DM mass $m_{DM} = 2$ TeV and life time $\tau \sim 1.08 \times 10^{26}$ s. The decay channels are the same as the annihilation scenario.

For pulsars, we adopt the spatial distribution parameters $a = 1.0$, $b = 1.8$ [35], and the power law index of the energy spectrum $\alpha \sim 1.4$ with an exponential cutoff above ~ 800 GeV. The spectrum index 1.4 can give good description to the Fermi data. However, to better fit the ATIC data we need to introduce harder spectrum and/or super-exponential cutoff.

The positron fraction and the total electron + positron flux are shown in Figure 1. The solar modulation effect is calculated using the force field approximation [37] with a potential of 500 MV in this work. For the background electron choice, we adopt the DC model given in Ref.[22]. A rescale factor 0.9 on the electron normalization is adopted to better fit the PAMELA and ATIC/Fermi data simultaneously. This model is actually similar with the so-called conventional model [38], which fits all the pre-Fermi CR data and is also successfully used to model the diffuse gamma-ray spectrum measured by Fermi at intermediate Galactic latitudes [39].

Finally we should point out that we take continuous distribution of the sources (pulsar or DM) to recover the PAMELA and ATIC/Fermi data in this work. Note that it is also possible that the locally observed electrons/positrons come from one or several nearby pulsars [17, 19] or DM clumps [40]. For the pulsar scenario, this assumption does not affect the discussion since the extrapolation to the whole Galaxy will hold regardless of how much the far pulsars can contribute to the local electron flux. For the annihilating DM model, although a single DM clump which is close enough to the Earth may be possible to give large boost factor, it is found to be of little probability to survive in a realistic DM distribution model [41, 42]. For the decaying DM scenario, since the “boost” effect from DM decay will be much weaker we will expect an even smaller probability to find a clump close and massive enough to explain the electron/electron data, compared with the annihilating DM scenario. Therefore the assumption of continuous distribution of sources is reasonable.

III. SYNCHROTRON RADIATION FROM THE THREE SCENARIOS

In this section we study the synchrotron emission from the primary electrons and positrons in the three scenarios to account for the locally observed cosmic e^\pm excesses. The predictions are based on the same configurations as discussed in the last section.

The synchrotron emissivity with frequency ν of a single electron with Lorentz factor γ in

a magnetic field B , is given as [43]

$$\epsilon(\nu, \gamma) = 4\sqrt{3}\pi r_e m_e c \nu_L x^2 \left\{ K_{4/3}(x) K_{1/3}(x) - \frac{3x}{5} [K_{4/3}^2(x) - K_{1/3}^2(x)] \right\} \text{ ergs s}^{-1} \text{ Hz}^{-1} \quad (8)$$

where $r_e = e^2/m_e c^2$ is the classical electron radius, $x \equiv \nu/(3\gamma^2 \nu_L)$ with $\nu_L = eB/2\pi m_e c$ the Lamor frequency, and $K_l(x)$ is the modified Bessel function of order l . For an ensemble of electrons/positrons with power law spectrum $\frac{dN}{dE} \propto E^{-\alpha}$, the corresponding synchrotron intensity is also a power law form $I(\nu) \propto \nu^{-\beta}$, with index $\beta = (\alpha - 1)/2$. The magnetic field strength in the Galaxy is adopted as [44]

$$B(R, z) = B_0 \exp\left(-\frac{R - R_\odot}{R_B}\right) \exp\left(-\frac{|z|}{z_B}\right), \quad (9)$$

where $R_B = 10$ kpc and $z_B = 2$ kpc, and the local magnetic field strength $B_0 = 5 \mu\text{G}$. Such a magnetic field can match the 408 MHz synchrotron longitude and latitude distributions [44].

Solving Eq. (1) we get the electron/positron distributions in the Galaxy. Then we can derive the synchrotron emissivity at any point in the Galaxy. The line of sight integral of the emissivity gives the synchrotron flux as a function of direction (l, b) , which can be compared with the observation.

A. Results from the three scenarios

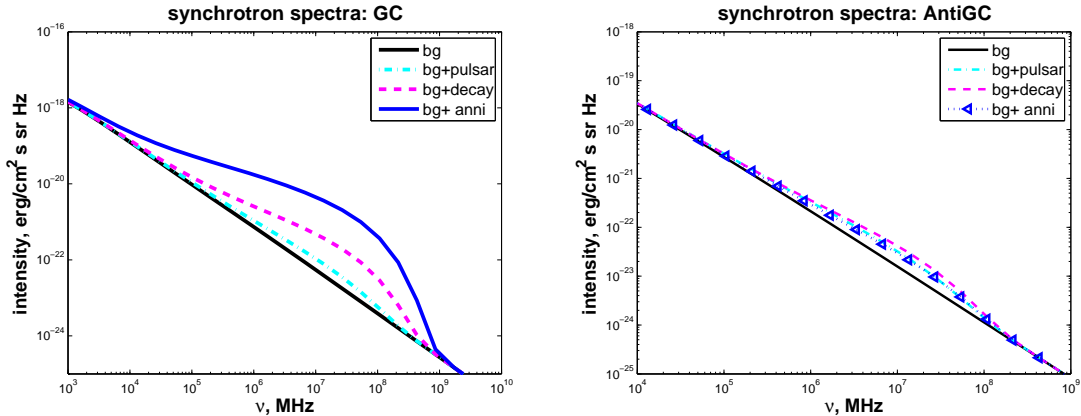


FIG. 2: The average synchrotron spectra of the three scenarios within a bin size of $20^\circ \times 20^\circ$ around GC and anti-GC, respectively.

In Figure 2, we give the average synchrotron spectra of the three different scenarios in a $20^\circ \times 20^\circ$ window centered at the Galactic center (GC) and anti-GC respectively. In the GC

direction the annihilating DM scenario has the largest signal, while in the anti-GC direction the decaying DM model has the largest signal though not very high in absolute fluxes. It is shown that these models have quite different synchrotron radiation spectra in the GC direction from 10^4 MHz to 10^9 MHz, even though they have similar contributions to the local electrons/positrons.

We give the results by smoothing the signals within the $20^\circ \times 20^\circ$ window centered at the GC so that we can diminish the uncertainties of our prediction. The largest uncertainty comes from the DM density profiles. The prediction of DM annihilation at the GC from cuspy or cored density profile may be orders of difference. By smoothing the signal within a large window the uncertainty is considerably decreased (see detailed discussion in Sec. 5). Further with a large window we can treat the pulsars as continuous distribution with average emission spectrum. Uncertainties from background are also decreased in a large window.

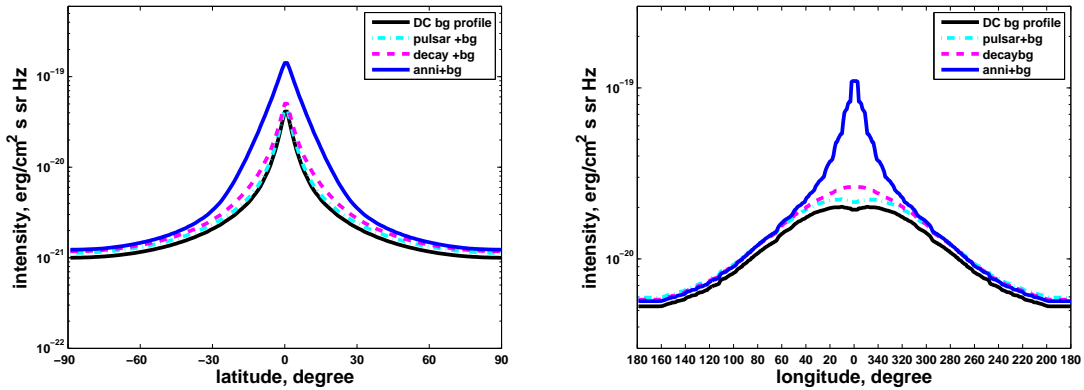


FIG. 3: The synchrotron latitude profile for $|l| < 10^\circ$ (left) and longitude profile for $|b| < 10^\circ$ (right), at the frequency of 61 GHz. The solid black line indicates the contribution from background electrons and positrons, and the other lines represent the total synchrotron intensities from the three scenarios together with the background respectively.

Given the large difference of synchrotron radiation from 10^4 MHz to 10^9 MHz in Figure 2, we choose a frequency randomly in this range, 61 GHz, to demonstrate the synchrotron longitude and latitude profiles in Figure 3. It is shown that the DM model will have larger gradient around GC, especially for the longitude profile, when compared with the pulsar model. For annihilating DM model the longitude profile is extremely cuspy around $l = 0$. This is a significant feature to distinguish among these models. In addition, the absolute

fluxes of the synchrotron radiation in the inner Galaxy are also different. For pulsar model, the longitude and latitude profiles almost follow the background distributions and might be difficult to be distinguished from the background. It is not hard to understand these profile features. The pulsar distribution is similar to the source distribution of CRs such as the supernova remnants, while the DM distribution is spherically symmetric and much more concentrated at GC than the pulsars. In addition the DM annihilation products are proportional to the square of DM density, $\rho^2(r)$, while the decay products depend only on the DM density $\rho(r)$. If the DM density is cuspy in the center of the halo, like that shown by many numerical simulations, the annihilation scenario will show the most cuspy profile at the GC direction.

B. The WMAP haze

The WMAP satellite has made all-sky survey in the microwave bands with several frequencies in the range $\sim 10 - 100$ GHz. The Galactic foreground dominates the radio emissions of these skymaps. Such emissions are expected to be produced by standard interstellar medium emission mechanisms, such as thermal dust, spinning dust, ionized gas and synchrotron radiation. After excluding all known contributions, however, Finkbeiner et al. reported an anomalous excess of the microwave emission around the GC which is called WMAP “haze” [25]. In Ref. [26], the authors confirmed the existence of the haze by analyzing WMAP three-year data and gave the possible implication of its origin. It is also proposed that the haze might come from the DM annihilation [45].

In Figure 4 we compare our calculated synchrotron profiles in the inner Galaxy from the three scenarios with the WMAP data. From this figure we can see that annihilating DM model may reproduce the WMAP haze data by taking proper density profile, while the decaying DM and pulsar models can not produce the steep rise toward the GC as shown in data.

IV. DIFFUSE γ -RAYS FROM IC SCATTERING

In this section we study the diffuse γ -ray emission in the same three scenarios as discussed in the last two sections. Diffuse γ -rays can be produced through IC scattering of energetic

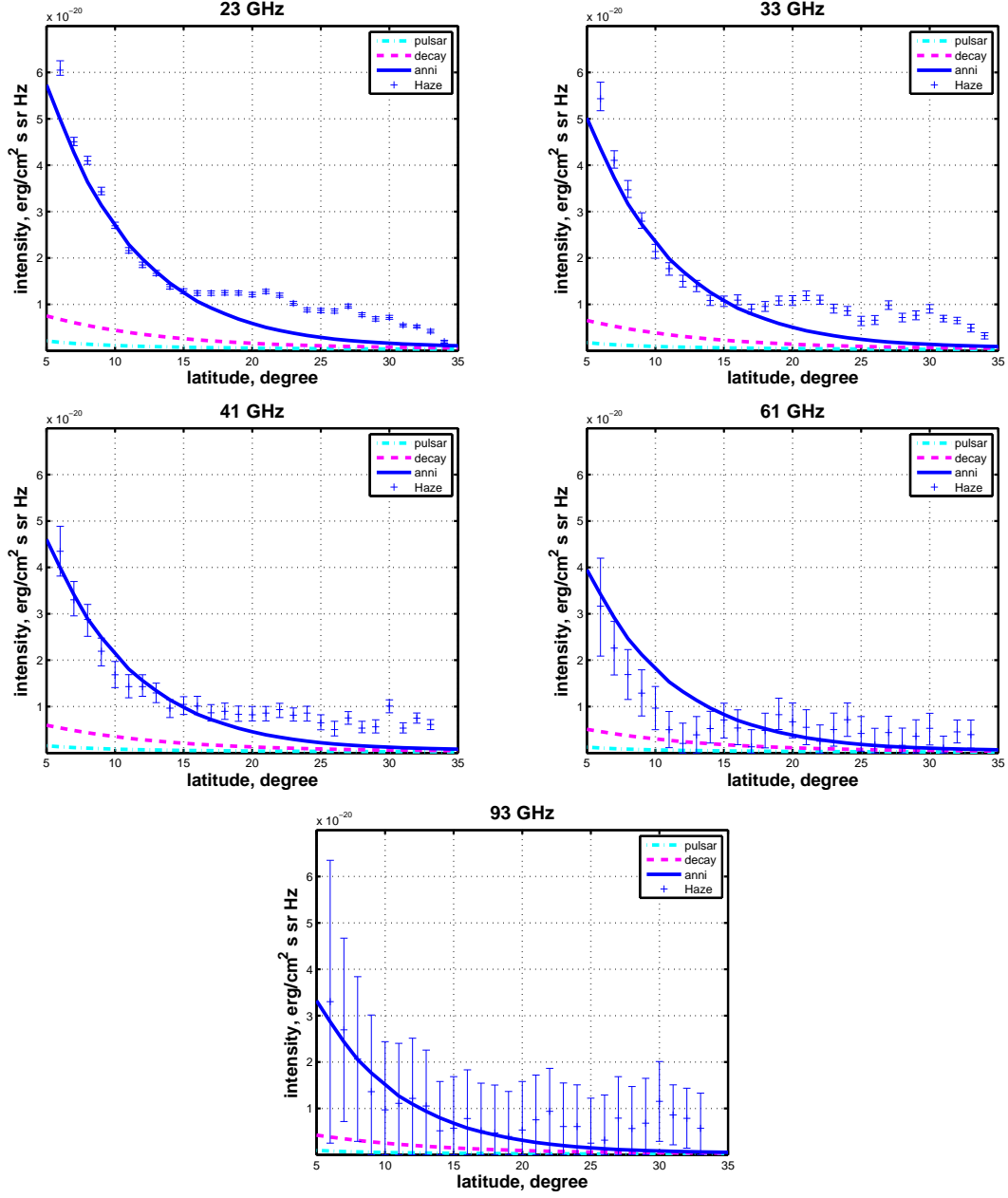


FIG. 4: Residual synchrotron intensities after subtracting the background for the three scenarios, compared with WMAP Haze data [26] at five different frequencies.

electrons and positrons with the interstellar radiation field (ISRF). The ISRF consists of radio emission of cosmic microwave background (CMB), infrared emission from dust and optical emission from stars. A model to calculate the ISRF distribution based on the realistic Galactic stellar and dust distributions was built by Porter and Strong [46] and this result has been included in the GALPROP package. In this work we use GALPROP to calculate

the IC-induced diffuse γ -rays generated by the primary electrons/positrons as well as the background diffuse γ -rays generated by conventional CRs [44]. Note that the final state gamma ray radiation of annihilating or decaying DM by internal bremsstrahlung, which is significant near the mass of DM, is not taken into account here. As shown in Ref. [10] the IC component will dominate the diffuse γ -rays in the Fermi energy range, which is also of major interest in this work.

In Figure 5, we show the diffuse γ -ray spectra for two sky regions, $|l| < 30^\circ, |b| < 5^\circ$ and $|l| < 60^\circ, |b| < 10^\circ$ for the three scenarios, corresponding to the region A [38] and region H [27] when discussing the EGRET data. The IC γ -rays from DM annihilation are significantly larger than the other two scenarios, especially for energies higher than several GeV. The contributions from pulsars are very small and almost undetectable if the uncertainties of the background are taken into account. The signal of decaying DM model is moderate. The results from all the three scenarios do not violate the observations of EGRET.

For comparison we also plot in Figure 5 the contributions of annihilating DM with Navarro-Frenk-White (NFW) profile,

$$\rho(r) = \frac{\rho_s}{\left[1 + \frac{r}{r_s}\right]^2}, \quad (10)$$

with $r_s = 20$ kpc and the local DM density $\rho_\odot = 0.3 \text{ GeV cm}^{-3}$ at $r = R_\odot \equiv 8.5 \text{ kpc}$. Since NFW profile is steeper in the halo center than Merritt profile, it will give harder γ -ray spectra. In a smaller sky region, the differences between these two kinds of DM distribution profiles are more obvious, as shown in Figure 6. We can see that the IC γ -rays and synchrotron radiation can provide a good test of the annihilating DM scenario and even give constraints on the inner profile of DM distribution [47, 48].

Figure 7 gives the diffuse γ -ray longitude and latitude profiles in the inner Galaxy, for two energy intervals, $4 - 10 \text{ GeV}$ and $10 - 100 \text{ GeV}$ respectively. The data points in the *top two panels* are from EGRET diffuse skymaps. It is shown that the precise measurements of the γ -ray gradient near GC will be also very helpful to discriminate different models, and possibly reveal the particle properties of DM [49].

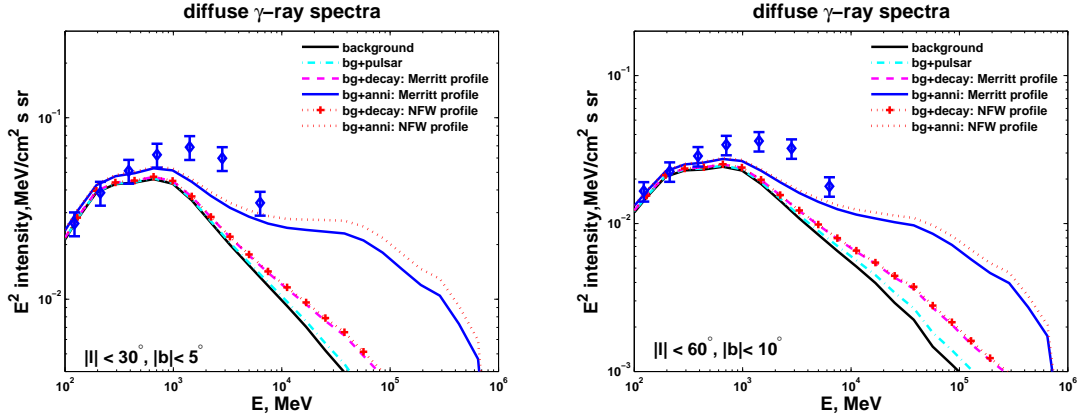


FIG. 5: The contributions to the diffuse γ -ray spectra in the inner Galaxy of the three scenarios for two sky regions, compared with the EGRET data [27].

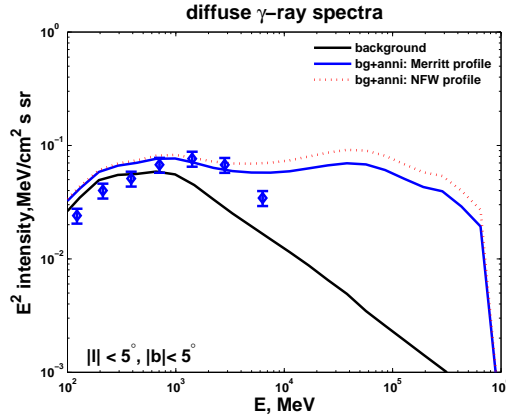


FIG. 6: Same as Figure 5 but for annihilation DM within a smaller region $|l| < 5^\circ, |b| < 5^\circ$. NFW and Merritt profiles are adopted to show the difference.

V. DISCUSSION ON THE UNCERTAINTIES OF PREDICTION

In the last two sections, we study the prospects to discriminate the three scenarios accounting for the PAMELA and ATIC data, i.e. annihilating DM, decaying DM and Galactic pulsars, through the synchrotron and IC radiation. For each scenario, a specific model is chosen. In this section we will discuss the uncertainties of the model configurations.

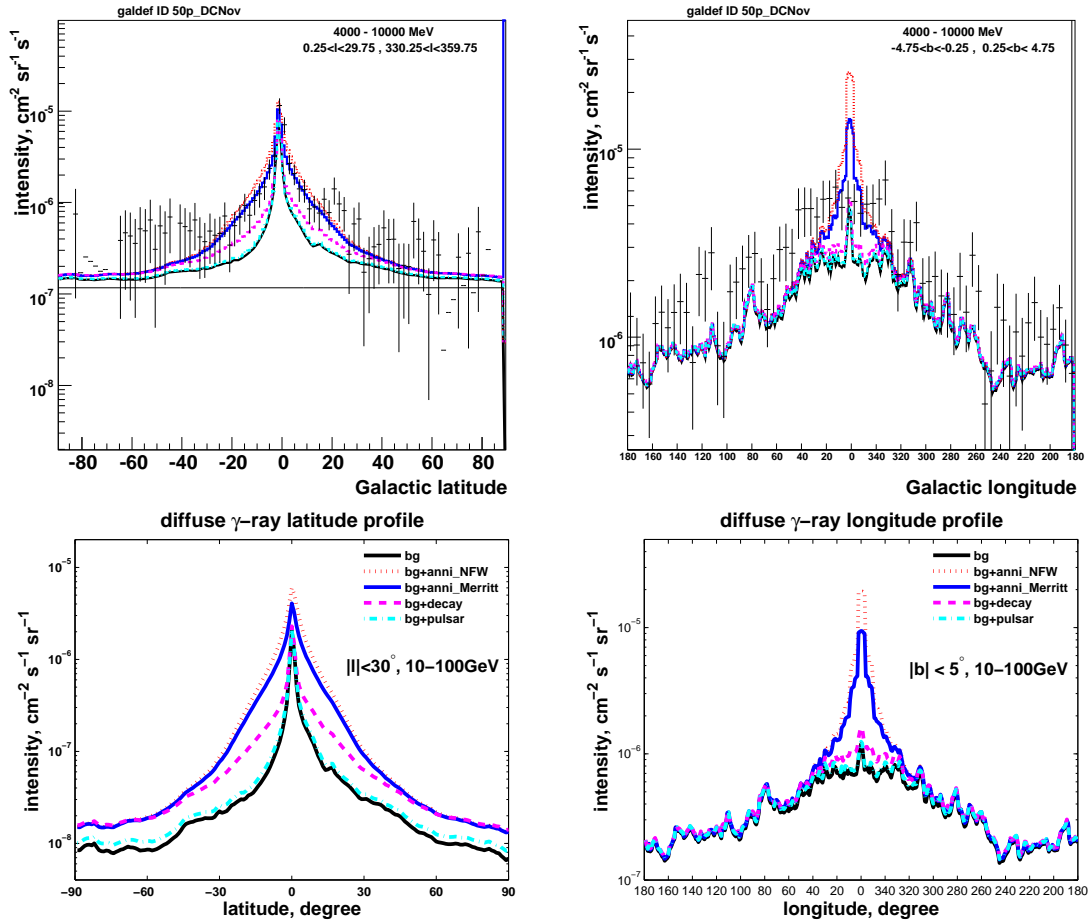


FIG. 7: The diffuse γ -ray latitude (average with $|l| < 30^\circ$) and longitude (average with $|b| < 5^\circ$) profiles. *Top two panels* are for energies 4 – 10 GeV, and the *bottom two panels* for 10 – 100 GeV.

A. Particle physics model of DM

In this work we adopt the annihilation/decay modes of DM only to leptons with equal branching ratios to e^+e^- , $\mu^+\mu^-$ and $\tau^+\tau^-$ to explain the PAMELA and ATIC data. However, our predictions of the synchrotron and IC radiation are not generally based on this specific choice. Since no matter how a model is constructed, the final electron and positron spectra have to be adjusted to fit the PAMELA and ATIC data. It is the electron and positron spectra that determine our prediction of the synchrotron and IC radiation.

Actually for a flavor blind DM the 1 : 1 : 1 branching ratios to e^+e^- , $\mu^+\mu^-$ and $\tau^+\tau^-$ is also the most natural and typical choice. First the PAMELA antiproton data severely constrained the gauge boson and quark final states [2]. As the first order approximation we

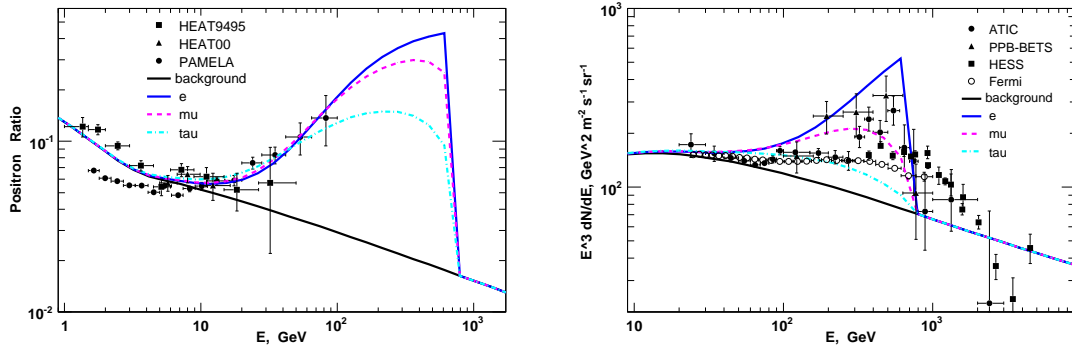


FIG. 8: The positron fractions and electron spectra in the case of pure e^+e^- , $\mu^+\mu^-$ or $\tau^+\tau^-$ final state of DM.

assume pure leptonic final states. Further, in Figure 8 we show that the PAMELA and ATIC data are not fitted very well if only e^+e^- , $\mu^+\mu^-$ or $\tau^+\tau^-$ final state is assumed. If we gauge the positron ratio to the PAMELA data, the electron/positron spectrum will be too hard to account for the ATIC data if only taking the e^+e^- channel, while it is too soft for the $\tau^+\tau^-$ channel. In addition, pure $\mu^+\mu^-$ or $\tau^+\tau^-$ could not reproduce the sharp falling at ~ 600 GeV at the ATIC spectrum. A combination of the three channels is necessary to account for the data from the two experiments simultaneously. The e^+e^- channel is mainly to produce the sharp falling at ATIC data while the $\tau^+\tau^-$ channel contributes to the PAMELA data at low energy.

According to the latest published data by Fermi [9] and HESS [8], the bump feature of electron spectrum is not as prominent as that observed by ATIC. In this case, the direct channel to e^+e^- to describe the fast drop of electron spectrum is not necessary. A DM model with purely $\mu^+\mu^-$ as the final states has been proposed to well fit the new data [11]. While from Fig. 8 we can see that a pure $\tau^+\tau^-$ channel might also be able to fit the Fermi/H.E.S.S. data. In the upper panels of Fig. 9 we show the positron fractions and total (e^+e^-) spectra from DM annihilation and decay, of which the final states have equal branching ratios into $\mu^+\mu^-$ and $\tau^+\tau^-$ ¹, such as in the gauged $L_\mu - L_\tau$ model [50]. In this calculation we adopt the same NFW DM density profile as in Eq.10, $m_{\text{DM}} = 1.5$ TeV for annihilation and $m_{\text{DM}} = 3$ TeV for decay. The predicted synchrotron and diffuse γ -ray spectra from the GC region are shown in the bottom panels of Figure 9. We can see from this figure that the annihilation

¹ A pure $\mu^+\mu^-$ or $\tau^+\tau^-$ channel can yield similar results, with the photon emission almost unchanged.

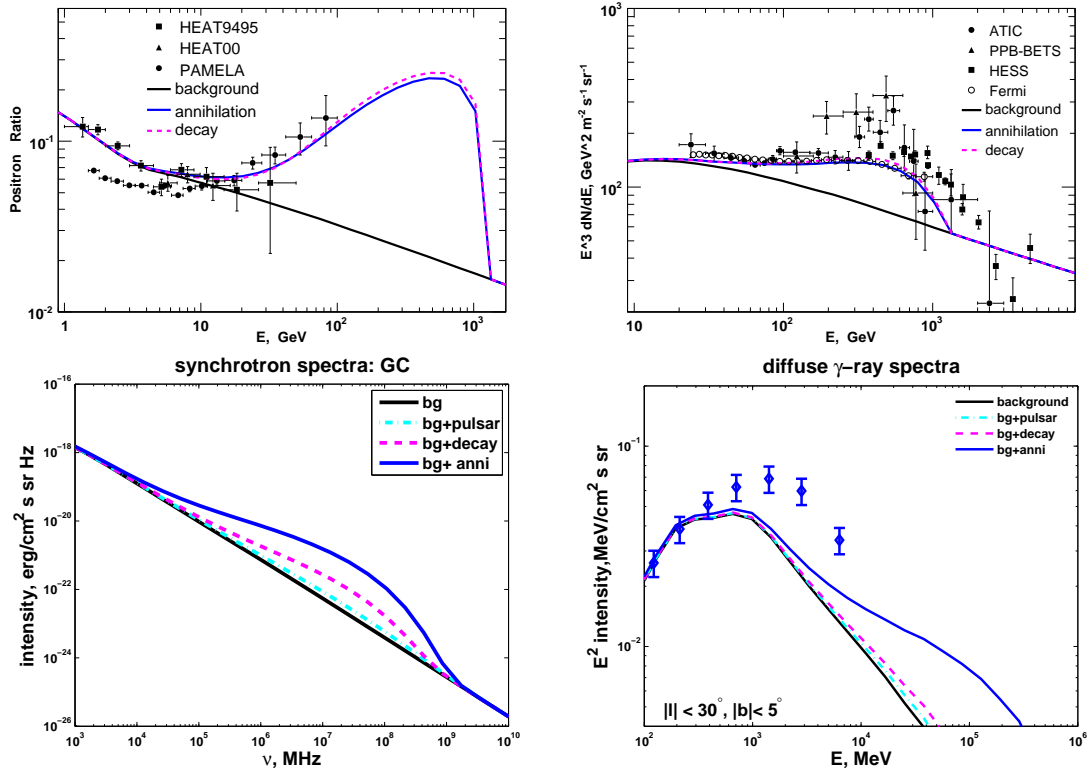


FIG. 9: The predictions of the positron fraction (upper-left), total ($e^+ + e^-$) spectrum (upper-right), synchrotron spectrum (bottom-left) and diffuse γ -ray spectrum (bottom-right) for a 1.5 TeV DM annihilation model and a 3 TeV DM decay model, both of which with equal branching ratios into $\mu^+\mu^-$ and $\tau^+\tau^-$. The pulsar scenario is the same as in Figures 2 and 5.

DM model could still be discriminated.

It should be noted that the current measurements of ATIC and Fermi are not fully consistent. Fermi result has high precision, however, both are dominated by systematic errors. The Fermi data seem to favor an astrophysical origin, such as from nearby pulsars. However, the ATIC data favor the DM scenario more. From our study we notice that the DM annihilation scenario seems always be distinguishable from the other two.

B. Spatial distribution of DM

The key point of the present work is that the three scenarios have quite different spatial distributions, especially near the Galactic center, although all the three scenarios are easily to account for the local measurements by PAMELA and ATIC. It may be difficult to

discriminate the three scenarios by local observations near the Solar system. However, the difference of the three scenarios near the GC should be large if we can try to observe their products, such as the synchrotron or IC radiation as we studied in this work. Therefore, the most important uncertainties should come from the spatial distribution of DM density.

In order to remove the uncertainties of the DM density profile we have averaged the synchrotron and IC radiation over a large window around the Galactic center. This will smooth the signals around the GC and diminish the uncertainties from DM density profile efficiently as well as the distribution of pulsars.

Numerical simulations generally suggest cuspy DM profiles in the center of the DM halo (e.g., [51, 52, 53]). In this work we adopt the Merritt profile with intermediate central density between the cuspy profiles like NFW and the cored one like isothermal. This DM profile gives a good description of the WMAP haze data, as shown in Figure 4.

To show the uncertainty of DM profile here we consider the most conservative case with the cored isothermal profile. The density profile is given as

$$\rho(r) = \frac{\rho_0}{1 + \left(\frac{r}{a}\right)^2}, \quad (11)$$

with $a = 5$ kpc and the local DM density $\rho_\odot = 0.3 \text{ GeV cm}^{-3}$ at $r = R_\odot \equiv 8.5$ kpc. With the same local density ρ_\odot , the cored isothermal profile is the least cuspiest distribution. Thus we anticipate it will produce the weakest photon signals at the GC. We show in Figure 10 the synchrotron spectra within a bin size of $20^\circ \times 20^\circ$ around the GC and the diffuse γ -ray spectra around the GC for cored isothermal DM profile compared with the pulsar model and the background. It is shown the differences between these models indeed become smaller compared with that given in Figure 2. The results shown in Figure 10 could be taken as the lower limit of our prediction, if other related models and parameters are fixed. Any other DM density profile will lead to a more clear discrimination of these predictions. In this conservative case with cored isothermal profile, it might be not easy to discriminate the DM signals.

C. Propagation model

Another source of uncertainties of our prediction comes from the propagation models. Actually requiring the propagation model to reproduce all the CR data gives strong con-

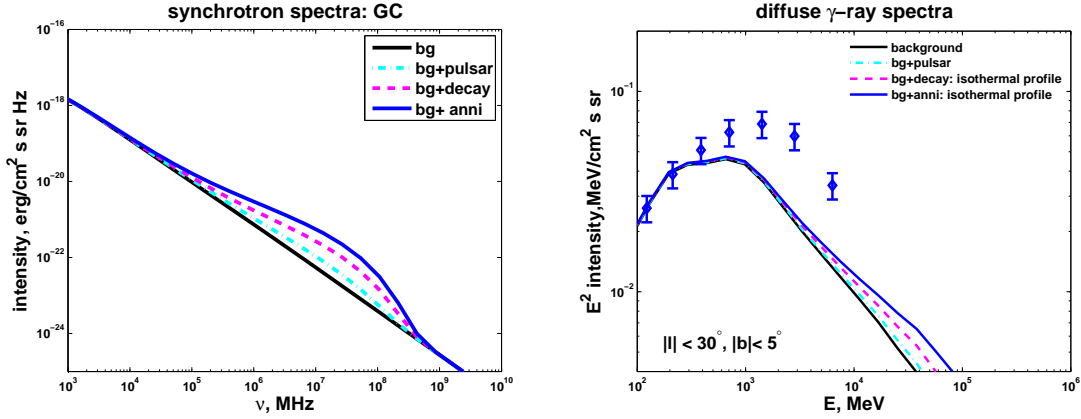


FIG. 10: The same as Figure 3 but for the isothermal DM profile.

constraints on the propagation parameters. The secondary to primary ratio, such as B/C , the unstable secondary to stable secondary, such as $^{10}\text{Be}/^9\text{Be}$, and the local proton, electron data are used to determine these parameters (see the discussion of the propagation model in Ref [22]). Under these requirement our results given in the previous sections will not change much by adjusting the propagation parameters, since the propagation models give similar descriptions to all kinds of CRs. Once other species satisfy data the model should also give similar electron and positron distributions at the same time. We will explicitly show the expectation in the following.

In the previous sections we adopt the conventional model that all the cosmic ray spectra are consistent with observations. We have ignored the effect of reacceleration in Eq. (1) and kept the effect of convection, which leads to better fit to the PAMELA data at low energies [22]. We will show in the following the propagation parameters will modify our results very slightly.

As an example we give the synchrotron spectra for diffusion + reacceleration (DR) propagation model adopting the same propagation parameters as in [22], which, contrary to the propagation model adopted in the present work, keeps the effect of reacceleration while ignores the effect of convection. In Figure 11 we plot the synchrotron spectra in the DR propagation model for the three scenarios to account for the PAMELA and ATIC data. We see that these results are almost the same as the prediction in the DC model shown in the left panel of Figure 2.

Another important uncertainty of propagation model comes from the height of the diffusion region. We have studied a propagation model with diffusion height 2kpc. The prop-

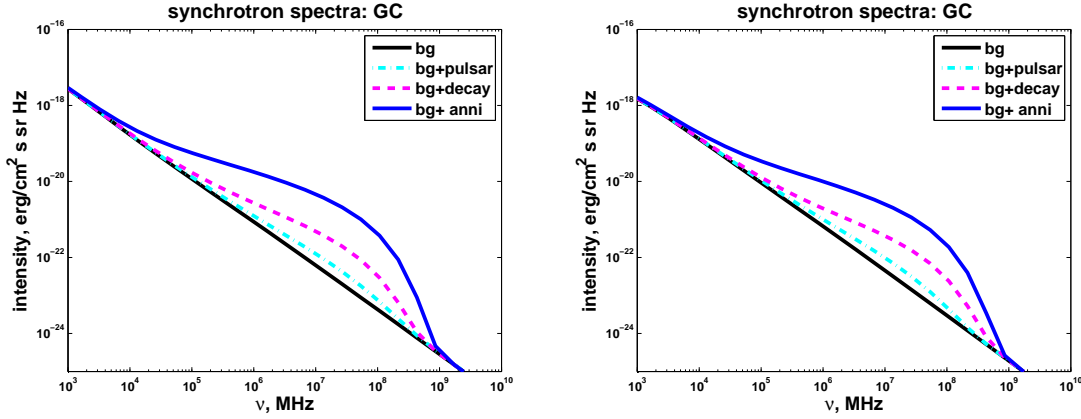


FIG. 11: The same as Figure 3 for *Left panel*: DR propagation model and *Right panel*: DC propagation model but with 2kpc diffuse halo height.

agation parameters are also adjusted to reproduce all the cosmic ray observations. In the right panel of Fig. 11 we show the synchrotron predictions in this 2kpc diffuse halo height propagation model. We see that the change of propagation parameters generally affect our predictions slightly.

D. Other astrophysical uncertainties

The synchrotron and IC radiation directly depend on the magnetic field and ISRF respectively. The GALPROP model has adopted the latest result of the magnetic field and ISRF, which are given according to the most recent astronomical observations. To fully figure out the uncertainties of these astronomical observations is not easy. However, taking these uncertainties into account will not change our conclusion in this work, since the change will affect all the three scenarios simultaneously. For example the strength of the magnetic field may have the uncertainty of a factor 2. To reduce the magnetic field twice will reduce all the synchrotron radiation of the three scenarios, together with the background, twice. This is equivalent to say that all the curves in the synchrotron plots should shift downwards, while the relative differences between these models are not changed. Similarly change of ISRF will shift the IC radiation for all the three scenarios at the same time. However, observations of radio or diffuse γ -rays by EGRET and Fermi especially at high latitude will constrain the magnetic field or ISRF that can not be too small.

VI. SUMMARY AND CONCLUSION

To explain the recent measurements of the positron fraction by PAMELA and electron spectrum by ATIC, Fermi and HESS, several scenarios including the DM and pulsars are proposed. In this paper we studied the perspective to discriminate these models using the synchrotron and IC radiation generated by these electrons/positrons. The point is that although various kinds of models degenerate in the local environment² and give similar electrons/positrons spectra, their different spatial extension might be revealed by the accompanied photon emission.

By properly adjusting the model parameters we first build three benchmark models which can reproduce the measured electron/positron data. We then studied the synchrotron and IC radiation from these primary electrons and positrons. We find that around the GC region, the synchrotron spectra for frequencies from $10^4 \sim 10^9$ MHz and the IC γ -ray spectra from several GeV to several hundred GeV are significantly different among the three scenarios, especially between annihilating DM scenario and others. For the directional profiles, the DM models show larger gradient near the GC, especially in the longitude profiles, than the pulsar model and the background. The photon emissions for pulsar model are very small and similar with the background, and will be the most difficult one to be detected. While for DM models, especially the annihilating DM model, there are strong observable signals. Finally we discuss the possible uncertainties of these conclusions. The major uncertainty comes from the DM inner profile. For the most conservative case with cored isothermal DM profile, the signals of DM scenarios become weaker and might be hard to be discriminated. However, the isothermal profile is generally disfavored by numerical simulations. Other uncertainties, such as the DM annihilation or decay channels, the propagation parameters and other astrophysical inputs, seems not to change the relative differences among the signals of the three scenarios significantly.

It should be pointed out that in this work the boost factor for the annihilating DM scenario is assumed to be universal, such as the Sommerfeld effect. It is also possible that the boost effect is spatially dependent, e.g., from the DM subhalos [29, 30, 31]. If so, the enhancement near the GC region will not be as important as at large radius in the halo.

² High energy electrons lose energy fast and the detected electrons should indeed be “local”, e.g., within ~ 1 kpc [54].

Actually, the calculation based on the N-body simulation indicates that the boost factor from DM substructure for anti-matter particles from DM annihilation in the Galaxy is generally negligible [32, 55]. A recent calculation on the DM clumpiness boost factor taking into account the Sommerfeld effect still finds no remarkable enhancement effect, except for fine tuning to the strongly resonant case [56]. Therefore the conclusions in this work are generally held.

Acknowledgments

We thank Prof. Fang-Jun Lu for helpful discussion on pulsars and PWNe. This work is supported in part by the Natural Sciences Foundation of China (Nos. 10773011, 10775001, 10635030), by the trans-century fund of Chinese Ministry of Education, and by the Chinese Academy of Sciences under the grant No. KJCX3-SYW-N2.

-
- [1] O. Adriani *et al.*, arXiv:0810.4995 [astro-ph].
 - [2] O. Adriani *et al.*, arXiv:0810.4994 [astro-ph].
 - [3] S. W. Barwick *et al.* [HEAT Collaboration], *Astrophys. J.* **482**, L191 (1997).
[arXiv:astro-ph/9703192].
 - [4] M. Aguilar *et al.* [AMS-01 Collaboration], *Phys. Lett. B* **646**, 145 (2007).
[arXiv:astro-ph/0703154].
 - [5] J. Chang *et al.*, *Nature* **456**, 362 (2008).
 - [6] S. Torii *et al.* [PPB-BETS Collaboration], arXiv:0809.0760 [astro-ph].
 - [7] H. E. S. S. Collaboration, arXiv:0811.3894 [astro-ph].
 - [8] F. Aharonian *et al.*, [H. E. S. S. Collaboration], arXiv:0905.0105 [astro-ph.HE].
 - [9] Fermi Collaboration, arXiv:0905.0025 [astro-ph.HE].
 - [10] I. Cholis, G. Dobler, D. P. Finkbeiner, L. Goodenough and N. Weiner, arXiv:0811.3641 [astro-ph].
 - [11] L. Bergstrom, J. Edsjo and G. Zaharijas, arXiv:0905.0333 [astro-ph.HE].
 - [12] D. A. Frail, M. F. Bietenholz, C. B. Markwardt, and H. Oegelman, *Astrophys. J.* **475**, 224 (1997)

- [13] G. G. Pavlov, O. Y. Kargaltsev, D. Sanwal, and G. P. Garmire, *Astrophys. J.* **554**, 189 (2001)
- [14] F. J. Lu, Q. D. Wang, B. Aschenbach, P. Durouchoux and L. M. Song, *Astrophys. J.* **568**, L49 (2002)
- [15] F. Aharonian *et al.* [H.E.S.S. Collaboration], *Astron. Astrophys.* **448**, L43 (2006) [arXiv:astro-ph/0601575].
- [16] X. H. Li, F. J. Lu and Z. Li, arXiv:0707.4279v2 [astro-ph].
- [17] D. Hooper, P. Blasi and P. D. Serpico, arXiv:0810.1527 [astro-ph].
- [18] H. Yuksel, M. D. Kistler and T. Stanev, arXiv:0810.2784 [astro-ph].
- [19] S. Profumo, arXiv:0812.4457 [astro-ph].
- [20] L. Bergstrom, T. Bringmann and J. Edsjo, arXiv:0808.3725 [astro-ph]. M. Cirelli and A. Strumia, arXiv:0808.3867 [astro-ph]; V. Barger, W. Y. Keung, D. Marfatia and G. Shaughnessy, arXiv:0809.0162 [hep-ph]; M. Cirelli, M. Kadastik, M. Raidal and A. Strumia, arXiv:0809.2409 [hep-ph]; N. Arkani-Hamed, D. P. Finkbeiner, T. Slatyer and N. Weiner, arXiv:0810.0713 [hep-ph]; M. Pospelov and A. Ritz, arXiv:0810.1502 [hep-ph]; I. Cholis, D. P. Finkbeiner, L. Goodenough and N. Weiner, arXiv:0810.5344 [astro-ph]; Y. Nomura and J. Thaler, arXiv:0810.5397 [hep-ph]; D. Feldman, Z. Liu and P. Nath, arXiv:0810.5762 [hep-ph].
- [21] C. R. Chen and F. Takahashi, arXiv:0810.4110 [hep-ph]; K. Ishiwata, S. Matsumoto and T. Moroi, arXiv:0811.0250 [hep-ph]; P. J. Fox and E. Poppitz, arXiv:0811.0399 [hep-ph]; C. R. Chen, F. Takahashi and T. T. Yanagida, arXiv:0811.0477 [hep-ph]; K. Hamaguchi, E. Nakamura, S. Shirai and T. T. Yanagida, arXiv:0811.0737 [hep-ph]; A. Ibarra and D. Tran, arXiv:0811.1555 [hep-ph]; C. R. Chen, F. Takahashi and T. T. Yanagida, arXiv:0811.3357 [astro-ph].
- [22] P. F. Yin, Q. Yuan, J. Liu, J. Zhang, X. J. Bi and S. H. Zhu, arXiv:0811.0176 [hep-ph].
- [23] E. Nardi, F. Sannino and A. Strumia, arXiv:0811.4153 [hep-ph].
- [24] M. Pohl, arXiv:0812.1174 [astro-ph].
- [25] D. P. Finkbeiner, *Astrophys. J.* **614**, 186 (2004) [arXiv:astro-ph/0311547].
- [26] G. Dobler and D. P. Finkbeiner, *Astrophys. J.* **680**, 1222 (2008) [arXiv:0712.1038 [astro-ph]].
- [27] S. D. Hunter *et al.*, *Astrophys. J.* **481**, 205 (1997).
- [28] A. W. Strong and I. V. Moskalenko, *Astrophys. J.* **509**, 212 (1998). [arXiv:astro-ph/9807150]; <http://galprop.stanford.edu/>
- [29] Q. Yuan and X. J. Bi, *JCAP* **0705**, 001 (2007) [arXiv:astro-ph/0611872].

- [30] X. J. Bi, J. Zhang, Q. Yuan, Phys. Rev. D **78**, 043001 (2008) [arXiv:0712.4038 [astro-ph]].
- [31] X. J. Bi, J. Zhang, Q. Yuan, J. L. Zhang and H. S. Zhao, Phys. Lett. B **668**, 87 (2008) [arXiv:astro-ph/0611783].
- [32] J. Lavalle, Q. Yuan, D. Maurin and X. J. Bi, Astron. Astrophys. **479**, 427 (2008). [arXiv:0709.3634 [astro-ph]].
- [33] D. Merritt, J. F. Navarro, A. Ludlow and A. Jenkins, Astrophys. J. **624**, L85 (2005) [arXiv:astro-ph/0502515].
- [34] I. Cholis, L. Goodenough and N. Weiner, arXiv:0802.2922 [astro-ph].
- [35] L. Zhang and K. S. Cheng, Astron. Astrophys. **368**, 1063 (2001)
- [36] S. Coutu *et al.*, *Prepared for 27th International Cosmic Ray Conference (ICRC 2001), Hamburg, Germany, 7-15 Aug 2001*
- [37] L. J. Gleeson and W. I. Axford, Astrophys. J. **154**, 1011 (1968).
- [38] A. W. Strong, I. V. Moskalenko and O. Reimer, Astrophys. J. **613**, 962 (2004) [arXiv:astro-ph/0406254].
- [39] D. Grasso *et al.* [FERMI-LAT Collaboration], arXiv:0905.0636 [astro-ph.HE].
- [40] D. Hooper, A. Stebbins and K. M. Zurek, arXiv:0812.3202 [hep-ph].
- [41] J. Lavalle, J. Pochon, P. Salati and R. Taillet, Astron. Astrophys. **462**, 827 (2007). [arXiv:astro-ph/0603796].
- [42] P. Brun, T. Delahaye, J. Diemand, S. Profumo and P. Salati, arXiv:0904.0812 [astro-ph.HE].
- [43] G. Ghisellini, P. W. Guilbert and R. Svensson, Astrophys. J. **334**, L5 (1988).
- [44] A. W. Strong, I. V. Moskalenko and O. Reimer, Astrophys. J. **537**, 763 (2000) [Erratum-ibid. **541**, 1109 (2000)] [arXiv:astro-ph/9811296].
- [45] D. Hooper, D. P. Finkbeiner and G. Dobler, Phys. Rev. D **76**, 083012 (2007) [arXiv:0705.3655 [astro-ph]]. G. Caceres and D. Hooper, Phys. Rev. D **78**, 123512 (2008) [arXiv:0808.0508 [hep-ph]].
- [46] T. A. Porter and A. W. Strong, arXiv:astro-ph/0507119.
- [47] G. Bertone, M. Cirelli, A. Strumia and M. Taoso, arXiv:0811.3744 [astro-ph].
- [48] L. Bergstrom, G. Bertone, T. Bringmann, J. Edsjo and M. Taoso, arXiv:0812.3895 [astro-ph].
- [49] T. E. Jeltema and S. Profumo, JCAP **0811**, 003 (2008) [arXiv:0808.2641 [astro-ph]].
- [50] X. J. Bi, X. G. He and Q. Yuan, arXiv:0903.0122 [hep-ph].
- [51] J. F. Navarro, C. S. Frenk and S. D. M. White, Astrophys. J. **490**, 493 (1997).

- [52] B. Moore, T. R. Quinn, F. Governato, J. Stadel and G. Lake, Mon. Not. Roy. Astron. Soc. **310**, 1147 (1999) [arXiv:astro-ph/9903164].
- [53] J. Diemand, B. Moore and J. Stadel, Nature **433**, 389 (2005).
- [54] D. Maurin and R. Taillet, Astron. Astrophys. **404**, 949 (2003) [arXiv:astro-ph/0212113].
- [55] J. Lavalley, E. Nezri, E. Athanassoula, F. S. Ling and R. Teyssier, Phys. Rev. D **78**, 103526 (2008) [arXiv:0808.0332 [astro-ph]].
- [56] Q. Yuan, X. J. Bi, J. Liu, P. F. Yin, J. Zhang and S. H. Zhu, arXiv:0905.2736 [astro-ph.HE].

